Dynamic fracture and spallation in ductile solids

J. N. Johnson

Citation: J. Appl. Phys. **52**, 2812 (1981); doi: 10.1063/1.329011
View online: http://dx.doi.org/10.1063/1.329011
View Table of Contents: http://jap.aip.org/resource/1/JAPIAU/v52/i4
Published by the American Institute of Physics.

Dynamic fracture and spallation in ductile solids

J. N. Johnson
Los Alamos Scientific Laboratory, Los Alamos, New Mexico 87545

(Received 19 September 1980; accepted for publication 16 December 1980)

A mathematical model of ductile hole growth under the application of a mean tensile stress is developed and applied to the problem of spallation in solids. The object is to describe dynamic ductile fracture under a wide range of tensile loading conditions. The mathematical model presented here describes both plate-impact spallation (as observed by postshot examination and time-resolved pressure measurements) and explosively produced spallation (as observed by dynamic x-radiographic techniques) in copper. It is found to be inapplicable to ductile fracture of expanding rings, even in the absence of possible adiabatic shear banding and classical necking instabilities, because of the fact that the mean tensile stress (void growth) and the deviatoric stress (homogeneous plastic shear strain) are not independent. A phenomenological model of void growth under uniaxial stress conditions is developed independently and applied to the numerical finite-difference solution of fracture in an expanding ring. The initial porosity in a material element is a random variable following Poisson statistics and the assumption that all the void radii are equal. The necessary theoretical generalizations and supporting experimental measurements to improve our understanding of fracture and fragmentation in expanding rings are discussed.

PACS numbers: 62.20.Mk, 62.50. + p, 81.40.Np, 46.30.Nz

I. INTRODUCTION

The term "spallation," as used in shock-wave research, is defined as planar separation of material parallel to the wave front as a result of dynamic tensile stress components perpendicular to this plane. The term "scabbing" has also been used to describe this phenomenon. Spallation in ductile materials is controlled by localized plastic deformation around small voids which grow and eventually coalesce to form the spall plane. Spallation in brittle materials takes place by dynamic crack propagation without large-scale plastic deformation (except perhaps in a very small region near the crack tip). The work presented here deals only with the former case in which the growth of voids within the material can be described by continuum theories of plastic flow.

In addition to spallation there is yet another important related fracture problem that we would like to be able to represent theoretically (perhaps with a *single* ductile fracture model that could also be used for spallation)—this is the case of radial fracture of expanding rings and shells.

The differences between (i) plate-impact-produced spallation, (ii) explosively produced spallation, and (iii) dynamic radial fracture in expanding shells, are illustrated in Fig. 1.

In Fig. 1A a flat impactor (of thickness δ) traveling at velocity u strikes a stationary target (of thickness $>\delta$). For symmetric impact (i.e., target and impactor are of similar materials), a compressive wave of amplitude $\frac{1}{2}\rho_0 Uu$ and duration $\sim 2\delta/U$ is generated in the target. Here ρ_0 is the initial density and U is the wave velocity in the impactor and the target. Interaction of this compressive wave with the free surface on the right produces a tensile stress $-\frac{1}{2}\rho_0 Uu$ at a distance δ from the free surface. If the magnitude and duration of this tensile stress are great enough, spallation occurs. This is the standard plate-impact spall experiment in which both the peak tensile stress and spall position are known *a priori*.

Figure 1B shows the development of the tensile stress produced by a high explosive in contact with the sample. The peak longitudinal compressive stress in this case is on the order of 200–300 kbars depending on the explosive and the sample. As the triangular-shaped stress wave is reflected from the free surface, a tensile wave of increasing negative amplitude is propagated back into the sample. At distance δ_1 from the free surface the tensile stress is $-p_1$, and at δ_2 it is $-p_2$. When the tensile stress becomes large enough (for a given tensile loading rate or for sufficiently long time), spallation occurs. Hence in this case the spall position and the tensile stress are not uniquely determined *a priori*, in contrast to the case of plate-impact spall. It becomes a somewhat more difficult matter to model explosively produced fracture.

In the case of ductile fracture of an expanding ring or shell, as shown in Fig. 1C, the process is even more complicated. After the passage and reverberation of the radial loading wave, the shell is given a mean outward velocity V_R which results in a uniform hoop strain rate $\dot{\epsilon}_{\theta\theta} \sim V_R/R$. The corresponding hoop stress depends on whether or not the material is flowing plastically. For elastic expansion $\sigma_{\theta\theta} \simeq (EV_R/R)t$, where E is Young's modulus and t is the time. Consider flaws f_1, f_2, and f_3 shown in Fig. 1C. These are weak spots that might be due to spatial variation in initial porosity, for example. As shown here, the weakest flaw is f_1 and will be the place at which fracture (void growth) begins. As the element containing flaw f_1 fails, release waves are sent out at speed c. Whether or not a nearby flaw undergoes catastrophic growth depends on its relative strength and its proximity to neighboring weak flaws.

The essential point of this discussion is that calculation of radial fracture in shells is even more difficult than that of spallation due to explosive loading, which in turn is more difficult than that of plate-impact spallation. In the simplest case the spall location and maximum possible tensile stress

 0021-8979/81/042812-14$01.10

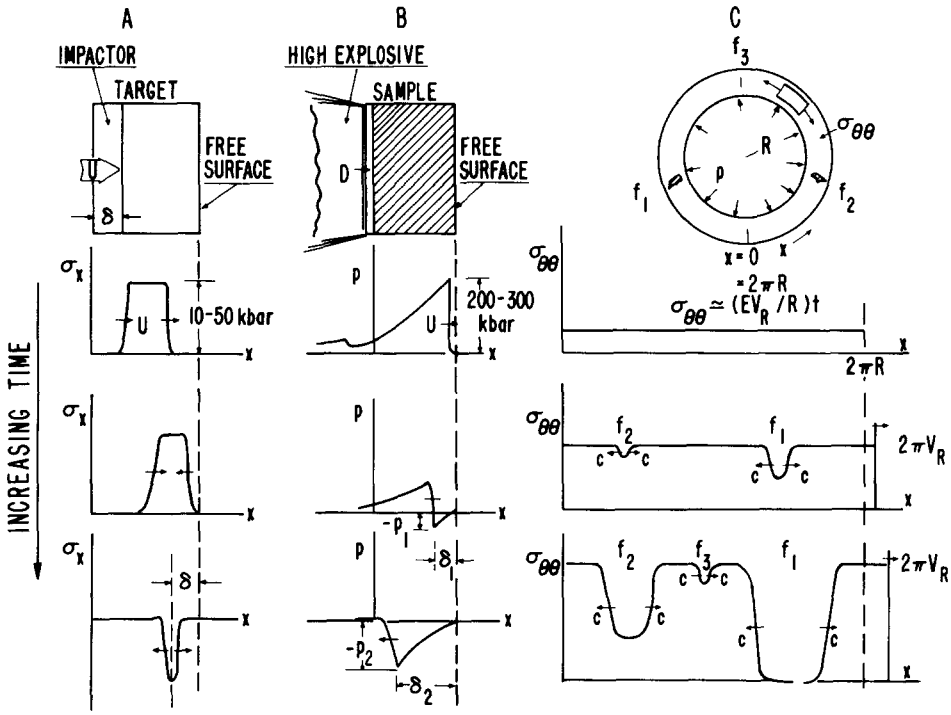

FIG. 1. Dynamic fracture for A, plate impact; B, explosive loading; and C, expanding ring.

are known *a priori*. In the second case (explosive loading) all that is known is the calculated tensile stress as a nondecreasing function of distance from the free surface (at least prior to the distance at which the tensile wave is fully formed and further hydrodynamic attenuation occurs as the reflected wave proceeds to the left). Neither the plate-impact nor the explosively loaded cases require statistical treatment of the various material elements in a calculation of the spall process: They are both entirely deterministic in nature. Radial fracture of shells must be calculated statistically since the detailed behavior shown in Fig. 1C depends on the statistical distribution of flaws, both in size and in spatial location on the circumference.

The study of spallation seems to begin with the early work of Hopkinson.[1] This was followed by a long period of relative inactivity until the work of Rinehart.[2–4] There then began (about 1960) an intense concentration of effort on this subject. McQueen and Marsh[5] measured the ultimate spall strength in copper for plate-impact conditions producing peak compressive pressures of 300–600 kbars. Similar high-pressure spall studies are reported by Skidmore.[6] Breed *et al.*[7] presented data on explosively produced spall in a number of metals.

Low-pressure spall thresholds in copper and the transition from incipient to complete failure was first studied by Smith,[8] followed by low-pressure spallation studies in other metals and numerous computational models of cumulative or partial damage.[9–15] Curran and co-workers[16–19] made detailed microscopic observation before and after shock-wave loading (both ductile and brittle solids) as a basis for nucleation and growth (NAG) models of spall fracture.

For every spallation experiment that is conducted, an *ad hoc* model can be developed to reproduce damage levels (in the form of residual porosity), spall location, growth rates, and so on. What is presently lacking is a single model of ductile fracture capable of reproducing the experimental results obtained under widely varying conditions. For example, in the work of Breed *et al.*[7] on explosively produced spallation of copper a computational model of fracture was developed to correlate spall strength with spall thickness. This model has been useful in reproducing the observed spall layers in explosive events, but is not applicable to low-pressure plate-impact experiments. Likewise, models developed for plate-impact situations seem to be inadequate in the high-pressure regime.[20] These models were developed to accurately represent the *onset* of fracture in engineering design and no serious attempt was made to see how they worked under the very extreme conditions of explosive loading at 200–300 kbars. The problem of fracture of expanding rings and shells has been considered from various points of view but no attempt has been made to relate it to spallation.[21–23]

Therefore models for the unified treatment of fracture processes must have sufficient generality to include the statistical distribution of one or more variables such as porosity, void density, etc. The NAG models[17–19] have this property but require numerous phenomenological constants that are difficult to obtain. The model of Cochran and Banner[15] is also based on statistical distributions of flaws, but is specifically written for use in a one-dimensional finite-difference code.

Therefore, in the present work, a microscopic model of ductile hole growth is developed which relates the material porosity (an internal state variable) to its initial value, the time history of the tensile pressure (or mean stress), and a single scalar parameter representing the rate-dependent plastic flow properties of the solid material surrounding the voids. This introduces a minimum number of adjustable parameters—also, the ones that are used have the possibility of

being determined experimentally. The model is expressed mathematically in a scalar (zeroth-order tensor) form, involving only the mean stress, that can be used in general multidimensional situations.

Finally, in recognition of the fact that currently important fracture problems involve reactive media, the influence of internal gas pressure (within the expanding voids) is included in the theory. In the present applications chemical reaction and ablation at the void surface are not considered. Theoretical results related to internal gas pressure, p_g are purely mechanical and are included here only for future reference.

II. VOID-GROWTH RELATIONS FOR DUCTILE MATERIALS

Carroll and Holt[24] describe a very useful model of void collapse in porous ductile materials that lends itself directly to a theory of void growth under tensile loading conditions—the only difference is that the pressure is negative in the void-growth case and the porosity increases. In spite of the obviously trivial replacement of p and $-p$ in the Carroll–Holt model, the complete derivation is repeated here since additional rate-dependent plastic flow terms and internal gas pressure are added that were not in the original development. The notation of Carroll and Holt is preserved as much as possible.

The derivation begins with the consideration of a rectangular volume element containing a representative distribution of voids as shown in Fig. 2. Imagine a uniform hydrostatic tension $\bar{p}$ acting over the surface of this element ($\bar{p}$ is assumed negative in tension). Throughout this work a bar over a variable will refer to macroscopic quantities averaged over the entire element, voids and all. Since the cross-sectional area occupied by the voids supports none of this stress, mechanical equilibrium requires that $A_s\bar{p}_s + (A - A_s)p_g = A\bar{p}$, where $\bar{p}_s$ is the mean stress (spatial average) in the solid material which subtends an average area A_s on plane of total area A and $p_g (\geqslant 0)$ is the internal gas pressure (for reactive media). For a random distribution of hole shapes and

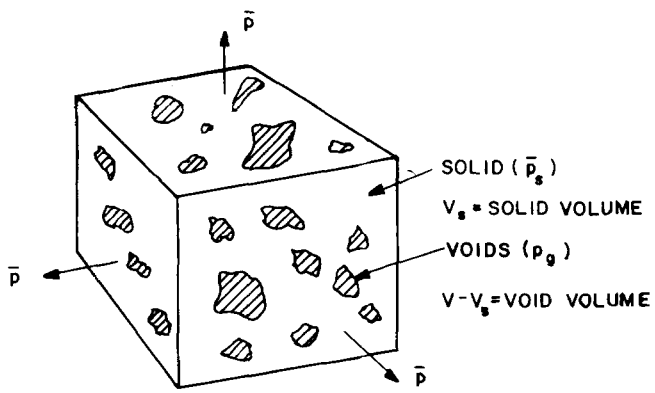

FIG. 2. Material element containing voids: $\bar{p}$ is the average mean stress acting over the element face, p_g is the gas pressure in the voids, and $\bar{p}_s$ is the average mean stress in the solid material.

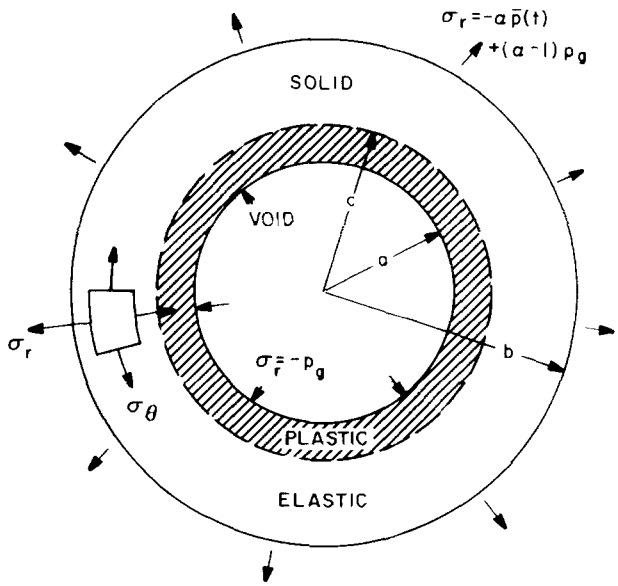

FIG. 3. Porous material model. The dimensions a and b are related to distension α.

sizes $(A_s/A) = (V_s/V)$ and we have that the mean stress in the solid constituent is[24]

$$\bar{p}_s = \alpha\bar{p} - (\alpha - 1)p_g, \tag{1}$$

where α, the distention ratio, is $(V/V_s) \geqslant 1$. Therefore around each of the voids in the distended material there is an average mean stress $\alpha\bar{p} - (\alpha - 1)p_g$. If this stress is big enough in tension (depending on the size of the holes), the voids will grow by plastic deformation in the surrounding solid matrix. The effect of positive internal pressure p_g is the same as an externally applied tensile pressure $\bar{p}$ (negative in tension).

A simplified model of the porous element is now assumed. Consider a single spherical void of radius a in a sphere of radius b subject to internal pressure p_g and external stress $\sigma_r = -\alpha\bar{p} + (\alpha - 1)p_g$ shown in Fig. 3. The essential point to the model is the following: *Relative values of a and b define the average porosity of the material and a_0 (the average initial hole size) becomes a material parameter.* Previous treatments of ductile hole growth[16,18] assumed that the applied tensile loading stress was applied at infinite external radius. One of the important consequences of the present assumption is that it leads naturally to a $\bar{p}$, α threshold relationship for fully plastic hole growth, as we shall see.

The relationship between a, b, and α is

$$\alpha = b^3/(b^3 - a^3) \tag{2}$$

or

$$(b/a)^3 = \alpha/(\alpha - 1). \tag{3}$$

The relationship between the distention α [or porosity $\phi = (\alpha - 1)/\alpha$] and the applied pressure $\alpha\bar{p}(t) - (\alpha - 1)p_g$ on the boundary is obtained by assuming that void expansion takes place with spherical symmetry such that the surrounding material does not change volume. In the spallation (void growth) process nearly all the volume change is associated with hole growth and very little with density changes in the solid constituent. This assumption was also made by

Cochran and Banner.[15] Let r_0 be the Lagrangian radial position coordinate in the solid surrounding the void and let r be the corresponding Eulerian coordinate. Then, in general,

$$r = f(r_0, t). \tag{4}$$

If the volume of the surrounding material is to be preserved, then $4\pi r^2 dr = 4\pi r_0^2 dr_0$ at each instant of time t. Thus

$$r^2\left(\frac{\partial r}{\partial r_0}\right)_t = r_0^2, \tag{5}$$

which has a solution

$$r^3 = r_0^3 - B(t), \tag{6}$$

where $B(t)$ is a function related to the rate of void growth. From Eq. (6) it is found that

$$\ddot{r} = \frac{\partial \psi}{\partial r}, \quad \psi(r,t) \equiv \frac{\ddot{B}(t)}{3r} + \frac{[\dot{B}(t)]^2}{18r^4}, \tag{7}$$

and

$$B(t) = a_0^3(\alpha_0 - \alpha)/(\alpha_0 - 1). \tag{8}$$

Thus

$B(t) > 0$, for $\alpha < \alpha_0$ (void compaction),

$B(t) < 0$, for $\alpha > \alpha_0$ (void growth).

Two useful relationships are

$$\frac{B(t)}{a^3} = \frac{\alpha_0 - \alpha}{\alpha - 1}, \quad \frac{B(t)}{b^3} = \frac{\alpha_0 - \alpha}{\alpha}. \tag{8a}$$

The equation of motion for material surrounding the void is given by

$$\rho \ddot{r} = \partial \sigma_r / \partial r + 2(\sigma_r - \sigma_\theta)/r, \tag{9}$$

where ρ is the solid density and σ_r and σ_θ are the radial and circumferential deviatoric stresses shown in Fig. 3. In this work, $\bar{p}$ is positive and σ_r, σ_θ are negative in compression according to the usual convention. Stress and strain variables without a bar refer to microquantities in the material surrounding the voids.

Substitution of Eq. (7) into (9) gives

$$\rho \partial \psi / \partial r = \partial \sigma_r / \partial r + 2\Delta s / r, \tag{10}$$

where $\Delta s \equiv \sigma_r - \sigma_\theta$. Equation (10) is then integrated from a to b with boundary conditions $\sigma_r(a,t) = -p_g$ and $\sigma_r(b,t) = -\alpha \bar{p} + (\alpha - 1)p_g$, to give

$$\rho[\psi_a(t) - \psi_b(t)] = -\alpha(\bar{p} - p_g) + 2\int_a^b \frac{\Delta s}{r} dr. \tag{11}$$

With the help of Eqs. (7) and (8), the left-hand side of Eq. (11) can be written as

$$\rho[\psi_a(t) - \psi_b(t)] = -\tau^2 Y_0 Q(\ddot{\alpha}, \dot{\alpha}, \alpha), \tag{12}$$

where Y_0 is the yield stress of the solid and

$$\tau^2 \equiv \rho a_0^2 / 3Y_0(\alpha_0 - 1)^{2/3}, \tag{13}$$

$$Q(\ddot{\alpha}, \dot{\alpha}, \alpha) \equiv -\ddot{\alpha}[(\alpha - 1)^{-1/3} - \alpha^{-1/3}] + \tfrac{1}{6}\dot{\alpha}^2[(\alpha - 1)^{-4/3} - \alpha^{-4/3}]. \tag{14}$$

Thus we have the following general relationship:

$$\tau^2 Y_0 Q(\ddot{\alpha}, \dot{\alpha}, \alpha) = \alpha(\bar{p} - p_g) - 2\int_a^b \frac{\Delta s}{r} dr. \tag{15}$$

Equation (15) is the relationship from which we obtain the rate-dependent response of void growth in spalling, ductile solids when specific expressions are substituted for Δs in the integrand on the right-hand side.

First consider elastic deformation in the small strain limit ($c < r < b$ in Fig. 3). The infinitesimal radial displacement is given by

$$u = r - r_0 \cong -B(t)/3r^2, \tag{16}$$

and the infinitesimal strain components (in the solid material surrounding the void) become

$$\epsilon_r = 2B(t)/3r^3, \quad \epsilon_\theta = -B(t)/3r^3. \tag{17}$$

Thus

$$\Delta s = 2GB(t)/r^3, \tag{18}$$

where G is the shear modulus of the solid.

In the plastic region ($a < r < c$ in Fig. 3) the material is initially assumed to be elastic perfectly plastic (this assumption will later be relaxed to include rate-dependent plastic flow):

$$\Delta s = (\sigma_r - \sigma_\theta) = \pm Y_0, \tag{19}$$

where Y_0 is the yield strength and the upper $+$ sign corresponds to void compaction (i.e., $\sigma_r > \sigma_\theta$) and the lower $-$ sign corresponds to void growth (i.e., $\sigma_r < \sigma_\theta$).

Plastic deformation begins at the inner ($r = a$) boundary (for void growth) when $\Delta s = 2GB(t)/a^3 = -Y_0$; that is, when

$$\hat{\alpha} = (2G\alpha_0 - Y_0)/(2G - Y_0). \tag{20}$$

If $\alpha_0 = 1.001$ (about 0.1% initial porosity from which the voids grow), $Y_0 \sim 1$ kbar, and $G \sim 200$ kbars, then $\hat{\alpha} = 1.001003$—very nearly equal to the initial distention. The spherical shell first becomes fully plastic when yielding occurs at the outer ($r = b$) boundary: $\Delta s = 2GB(t)/b^3 = -Y_0$, or

$$\hat{\hat{\alpha}} = 2G\alpha_0/(2G - Y_0). \tag{21}$$

For the same material parameters considered above, $\hat{\hat{\alpha}} = 1.0035$, which corresponds to a porosity very small in comparison to those expected in the latter stages of hole growth.

Therefore an important and useful simplification can be made when calculating complete or nearly complete fracture. *When dealing with void growth in materials of very low initial porosities, we can neglect the initial elastic and elastic-plastic phases of the process and go immediately to the case of fully plastic deformation around the void.* This may not always be the case, however, as in calculations of very low spallation porosities ($\alpha \simeq 1$), for example.

In addition, a rate-dependent contribution is added to the shear deformation and Eq. (19) is modified to give

$$\Delta s = (\sigma_r - \sigma_\theta) = \pm Y_0 + \frac{d}{\hat{b}^2 N}\dot{\gamma}^p, \tag{22}$$

where $\hat{b}$ is the Burgers vector, N is the mobile dislocation density, D is the drag coefficient, and $\dot{\gamma}^p$ is the plastic shear strain rate. For large finite strains the radial displacement is found from Eq. (6) to be

$$u = r - r_0 = r - [r^3 + B(t)]^{1/3} \tag{23}$$

and,consequently,

$$\gamma^p = \frac{\partial u}{\partial r} - \frac{u}{r} = -\left(1 + \frac{B(t)}{r^3}\right)^{-2/3} + \left(1 + \frac{B(t)}{r^3}\right)^{1/3}. \tag{24}$$

Since the motion takes place at constant volume, all of the strain can be considered plastic once yielding has occurred. Hence, by differentiation of Eq. (24),

$$\frac{\dot{\gamma}^p}{r} = \frac{\dot{B}(t)}{r^4}\left[\tfrac{2}{3}\left(1 + \frac{B(t)}{r^3}\right)^{-5/3} + \tfrac{1}{3}\left(1 + \frac{B(t)}{r^3}\right)^{-2/3}\right] \tag{25}$$

and, from Eqs. (2), (22), and (25),

$$2\int_a^b \frac{\Delta s}{r} dr = \pm \frac{2Y_0}{3}\ln\left(\frac{\alpha}{\alpha - 1}\right) + \frac{2D}{3\hat{b}^2 N}\frac{\dot{\alpha}}{\alpha(\alpha - 1)}F(\alpha,\alpha_0), \tag{26}$$

where

$$F(\alpha,\alpha_0) = \alpha\left(\frac{\alpha - 1}{\alpha_0 - 1}\right)^{2/3} - (\alpha - 1)\left(\frac{\alpha}{\alpha_0}\right)^{2/3} \cong \alpha\left(\frac{\alpha - 1}{\alpha_0 - 1}\right)^{2/3}, \quad \text{for } (\alpha_0 - 1) \ll 1. \tag{27}$$

Substitution of Eq. (26) into Eq. (15) gives

$$\tau^2 Y_0 Q(\ddot{\alpha},\dot{\alpha},\alpha) = \alpha(\bar{p} - p_g) \mp \frac{2Y_0}{3}\ln\left(\frac{\alpha}{\alpha - 1}\right) + \eta\frac{\dot{\alpha}}{\alpha(\alpha - 1)}F(\alpha,\alpha_0), \tag{28}$$

where $\eta = 2D/3\hat{b}^2 N$.

Assume that the terms involving $\ddot{\alpha}$ and $\dot{\alpha}$ are small and that $p_g = 0$. Thus

$$p_{eq}(\alpha) = \pm (2Y_0/3\alpha)\ln[\alpha/(\alpha - 1)]. \tag{29}$$

This is the equilibrium path followed for either void expansion (−) or compaction (+) at slow rates of loading. The term "slow" is meant here to mean that the quantities $\alpha\bar{p}$ and $(\frac{2}{3}Y_0)\ln[\alpha/(\alpha - 1)]$ in Eq. (28) are both large compared with those involving τ and η. A hypothetical tension/compression process is shown diagrammatically in Fig. 4, where $\bar{p}$ is plotted as a function of $\alpha - 1$. Starting at point 1 with $p = 0$ and $\alpha = \alpha_0$, the material is taken into tension (without change of α) until the P_{eq} curve is reached at point 2. Voids then grow and the absolute magnitude of the tensile (negative) pressure that can be supported is reduced as the $\bar{p}$, α state goes from point 2 to point 3. At point 3 the remaining tensile pressure is relieved and the material compressed to point 4 where the reverse yielding occurs. The porosity that is created in going from point 2 to point 3 is partially eliminated as the material is compacted from point 4 to point 5.

The symmetry of the $\pm p_{eq}$ curves about the $\alpha - 1$ axis raises an interesting question. In spallation experiments, the spall plane initially experiences a maximum compressive stress of approximately the same magnitude as tensile state 2 depicted in Fig. 4. This suggests that the material state could never reach the $-p_{eq}$ curve in a spallation experiment; i.e., the precompression would reduce the distention to a value such that the later tension would not be sufficient to cause void growth. This conclusion is contrary to what is known

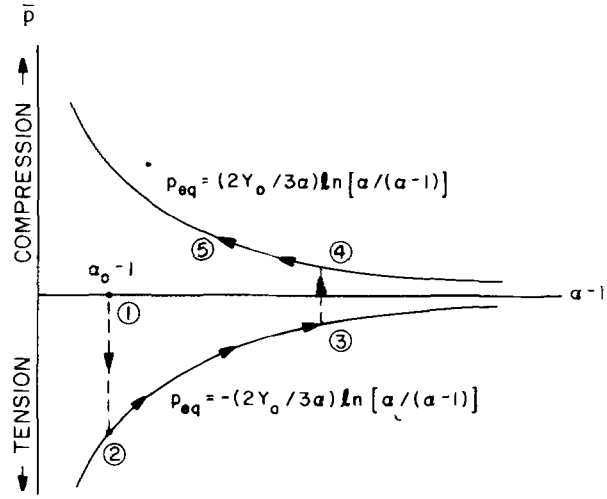

FIG. 4. Slow (equilibrium) tension-compression path in material with initial distension α_0 [porosity $= (\alpha_0 - 1)/a_0$].

about spallation in ductile materials—namely, (i) ductile metals *do* undergo spallation following an initial compression, (ii) precompression does not significantly change the spallation threshold,[11] and (iii) ductile void growth plays an important part in the initial stages of dynamic ductile fracture.[13,16,18] Therefore the initial distention α_0 might be thought of as an *effective* distention caused by solid inclusions (that cannot be eliminated by precompression), for example. These inclusions would necessarily have to be weakly bonded to the surrounding material in order that $\sigma_r(a,t) \cong 0$ (inert case) in the prototype model of void growth described here. This also raises interesting questions regarding the possibility of placing artificial spherical inclusions weakly bonded within well-understood ductile materials to verify the present model of ductile void growth.

To interpret the rest of the terms in Eq. (28), it is written as

$$\underset{\substack{\text{inertial}\\\text{resistance}\\\text{to void}\\\text{growth}}}{\tau^2 Y_0 Q(\ddot{\alpha},\dot{\alpha},\alpha)} - \underset{\substack{\text{resistance}\\\text{to plastic}\\\text{flow}}}{\eta\frac{\dot{\alpha}F(\alpha,\alpha_0)}{\alpha(\alpha - 1)}} = \underset{\substack{\text{driving}\\\text{stress}}}{\alpha\Delta p}, \tag{30}$$

where

$$\Delta p \equiv \bar{p} - p_g - p_{eq}(\alpha) \tag{31}$$

and $p_{eq}(\alpha)$ is given by Eq. (29). Equation (30) applies for $\bar{p} < p_{eq}(\alpha)$ in tension or $\bar{p} > p_{eq}(\alpha)$ in compression. Otherwise, $\dot{\alpha} \equiv 0$. The first term on the left-hand side of Eq. (30) represents inertial resistance to void growth and is proportional to the density of the solid surrounding the voids. This term vanishes when $\dot{\alpha}$ and $\ddot{\alpha}$ are zero. Even in the case of ideal rate-independent plastic flow in the solid material surrounding the voids ($\eta = 0$) there is a rate-dependent relationship between void growth and the driving stress. This depends specifically on the relaxation time τ given in Eq. (13). For example, if $\rho = 8.9$ g/cm^3 (copper), $Y_0 = 0.001$ Mbar, $a_0 = 10^{-4}$ cm, and $\alpha_0 - 1 = 0.001$, we find $\tau \sim 50$ ns.

Thus τ is small and void growth may be dominated by rate-dependent plastic flow rather than inertial effects. Since it is difficult to ascribe clear physical significance to the parameter τ, this conjecture can be better tested by comparing the relative magnitudes of the two terms on the left-hand side of Eq. (30). For typical materials[25] $D \sim 10^{-4}$ dyne s/cm^2, and therefore $\eta \sim 10^3$ dyne s/cm^2. With $\dot{\alpha} = 10^{-2}\,\mu s^{-1}$, $\ddot{\alpha} = 0$, and the remaining parameters as given in the previous paragraph:

$$\tau^2 Y_0 Q(o,\dot{\alpha},\alpha_0) \sim 5 \times 10^{-7} \text{ Mbars},$$

$$\eta\dot{\alpha}/[\alpha_0(\alpha_0 - 1)] \sim 10^{-2} \text{ Mbars}.$$

Thus, with some fairly reasonable values of η, etc., it seems that rate-dependent void growth can be initially dominated by plastic flow rather than inertial effects, at least in some specific instances. This is certainly not meant to be a general conclusion. Each case must be investigated individually.

Therefore the simplified model for ductile hole *growth* is written, for $p_g = 0$,

$$\dot{\alpha} = 0, \Delta p \geqslant 0$$

$$\dot{\alpha} = -\frac{(\alpha_0 - 1)^{2/3}}{\eta}\alpha(\alpha - 1)^{1/3}\Delta p, \quad \Delta p < 0 \tag{32}$$

$$\Delta p \equiv \bar{p} + \frac{a_s}{\alpha}\ln\frac{\alpha}{\alpha - 1},$$

where the constant a_s has replaced $\frac{2}{3} Y_0$, and the approximation given by Eq. (27) is used. In the calculations of this paper a_s is assumed to be a material parameter independent of the yield strength used in the macroscopic wave-propagation calculations. This seems justified because of the large amount of work hardening and temperature increase that occur in the vicinity of a growing void in comparison to uniaxial-strain shock-wave compression.

In the case that inertial effects are included, Eq. (30) is used in conjunction with Δp of Eq. (32).

III. ONE-DIMENSIONAL FINITE-DIFFERENCE CALCULATIONS

The one-dimensional flow equations in terms of the Lagrangian position coordinate x are

$$\frac{\partial \bar{\epsilon}}{\partial t} + \frac{\partial \dot{\bar{u}}}{\partial x} = 0, \quad \bar{\epsilon} \equiv 1 - \frac{\bar{\rho}_0}{\bar{\rho}} \tag{33}$$

$$\bar{\rho}_0 \frac{\partial \dot{\bar{u}}}{\partial t} - \frac{\partial \bar{\sigma}}{\partial x} = 0, \tag{34}$$

$$\bar{\rho}_0 \frac{\partial \overline{E}}{\partial t} - \bar{\sigma}\frac{\partial \dot{\bar{u}}}{\partial x} = 0, \tag{35}$$

where t is the time, $\bar{\rho}$ is the density ($\bar{\rho}_0$ = initial density), $\dot{\bar{u}}$ is the particle velocity in the x direction, $\bar{\sigma}$ is the longitudinal stress component, and $\overline{E}$ is the internal energy per unit mass. As stated previously, a bar over a variable indicates a macroscopic value, i.e., one averaged over void and solid. These equations are written in centered finite-difference form, combined with a material constitutive equation, and solved numerically to give the stress, particle-velocity, and void-growth histories in a shock-loaded sample undergoing spallation.

The material constitutive equation is written in terms of the mean stress (pressure) $\bar{p}$ and the deviatoric stress components $\bar{s}_{ij}$. in the model described here, void growth is related only to $\bar{p}$. The deviatoric stress components depend on the shear modulus $\overline{G}$ and the yield strength $\overline{Y}$, which are each functions of porosity. The plastic yield condition for the solid is

$$\tfrac{3}{2}\bar{s}_{ij}\bar{s}_{ij} = \overline{Y}^2 = (Y_0/\alpha)^2. \tag{36}$$

No attempt is made to include a rate-dependent term of the type used in Eq. (22) for calculations of wave profiles. These effects are still poorly understood themselves and do not greatly influence the fracture process. Nothing is claimed in this paper about the quantitive correctness of shock rise times and other macroscopic elastic-plastic rate effects of plane-wave propagation.

In the elastic region ($3\bar{s}_{ij}\bar{s}_{ij} < 2\overline{Y}^2$) the stress deviator rates are given by

$$\dot{\bar{s}}_{ij} = 2\overline{G}(\dot{\bar{\epsilon}}_{ij} - \tfrac{1}{3}\delta_{ij}\dot{\bar{\epsilon}}). \tag{37}$$

In the absence of porosity, the pressure-volume response is represented in terms of the high-pressure straight-line U_s (shock speed), U_p (particle velocity) relationship:

$$U_s = c_0 + sU_p, \tag{38}$$

where c_0 is the low-pressure bulk sound speed $(K_0/\rho_0)^{1/2}$, K_0 is the adiabatic bulk modulus at zero pressure, and s is a nondimensional constant. The Mie-Grüneisen equation of state for solids of this type is given by (in the absence of porosity the bars are removed from the variables ρ, ρ_0, ϵ, etc. without ambiguity)

$$p = \frac{K_0(1 - \frac{1}{2}\Gamma_0\epsilon)}{(1 - s\epsilon)^2} + \rho\Gamma E, \tag{39}$$

where Γ is the Grüneisen coefficient (here $\rho\Gamma$ is assumed to be a constant given by its low-pressure value $\rho_0\Gamma_0$). The time derivative (at constant x) of Eq. (39) is

$$\dot{p} = K_0\frac{(1 + s\epsilon - \Gamma_0\epsilon)}{(1 - s\epsilon)^3}\dot{\epsilon} + \rho_0\Gamma_0\dot{E}. \tag{40}$$

Equation (40) applies to solids for which there is no permanent inelastic volume strain. For void growth this is not the case. The plastic opening of voids results in an inelastic volume strain increment given by $-d(V - V_s)/V$ (see Fig. 1), which becomes $-\dot{\alpha}/\alpha$ when V_s remains constant, as assumed in the plastic model of void growth. The elastic, or recoverable, part of the total strain $\bar{\epsilon}$ is then $\epsilon^e = \bar{\epsilon} + \ln\alpha$ which alone is capable of supporting a pressure. Therefore when voids are growing Eq. (40) must be replaced by

$$\dot{\bar{p}} = \frac{\overline{K}(1 + s\epsilon^e - \Gamma_0\epsilon^e)}{(1 - s\epsilon^e)^3}\left(\dot{\bar{\epsilon}} + \frac{\dot{\alpha}}{\alpha}\right) + \bar{\rho}_0\overline{\Gamma}_0\overline{E}. \tag{41}$$

The (macroscopic) moduli $\overline{G}$ and $\overline{K}$ are assumed to be degraded by the presence of voids according to a model suggested by Mackenzie[26]:

$$\overline{K} = 4G_0K_0(1 - \phi)/(4G_0 + 3K_0\phi), \tag{42}$$

$$\overline{G} = G_0(1 - \phi)\left(1 - \frac{6K_0 + 12G_0}{9K_0 + 8G_0}\phi\right). \tag{43}$$

where K_0 and G_0 are the elastic moduli of undistended material and $\phi = (\alpha - 1)/\alpha$ is the porosity. Equation (43) agrees

exactly with Mackenzie's result for $\phi \ll 1$, but has been modified here such that $\bar{G}$ goes to zero as ϕ approaches unity. It is also required that $(6K_0 + 12G_0) \leqslant (9K_0 + 8G_0)$ to satisfy the stability condition $\bar{G} \geqslant 0$.

IV. PLATE-IMPACT AND EXPLOSIVELY GENERATED SPALL IN COPPER

As an application of the foregoing theory, two quite different spallation experiments on copper are calculated. The first is a plate-impact experiment[18] in which a 0.6-mm-thick copper plate strikes a 1.6-mm copper target backed by a relatively thick plate of PMMA (polymethylmethacrylate) in which a manganin pressure gauge is embedded approximately 0.5 mm from the copper (target)/PMMA interface. The impact velocity of 0.016 cm/μs produces a 29-kbar peak stress in the copper. The reason for choosing this particular experiment is that postshot photomicrographic observations of the residual porosity are available, and that the stress amplitude (29 kbars) and pulse duration (~ 0.3 μs) are sufficiently great to produce substantial porosity ($\sim 30\%$) at the spall plane. The experimental setup and the manganin pressure gauge record are shown in Fig. 5. The effect of spallation in the copper target is first detected by the gauge at a time between 0.8 and 0.9 μs after impact. The dashed line in Fig. 5 denotes the hypothetical record that would have been obtained if the sample had *not* spalled.

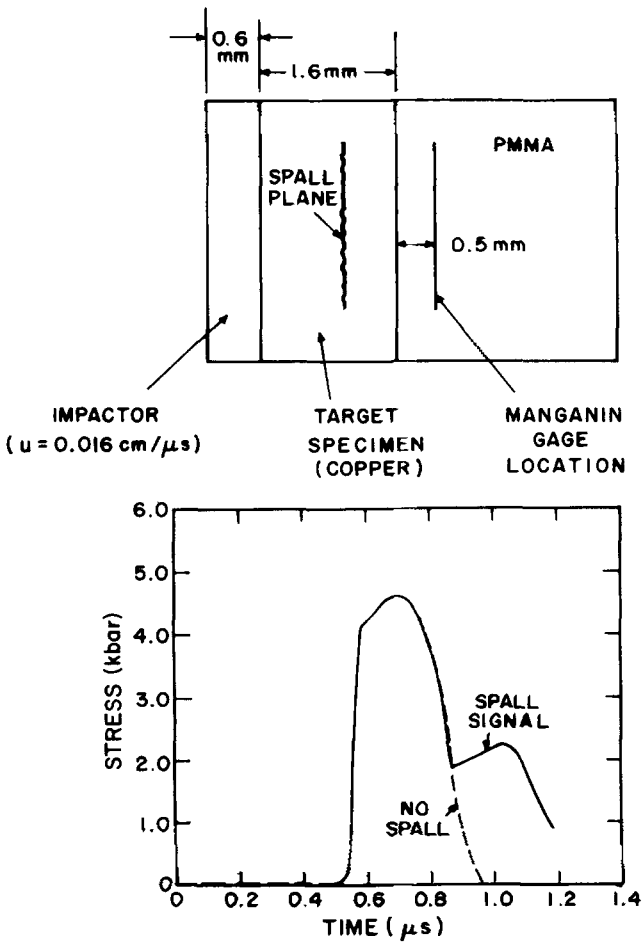

FIG. 5. Plate-impact test (SRI-S24) on copper backed with polymethylethacrylate (PMMA) containing manganin pressure gauge (gauge record shown on botton).

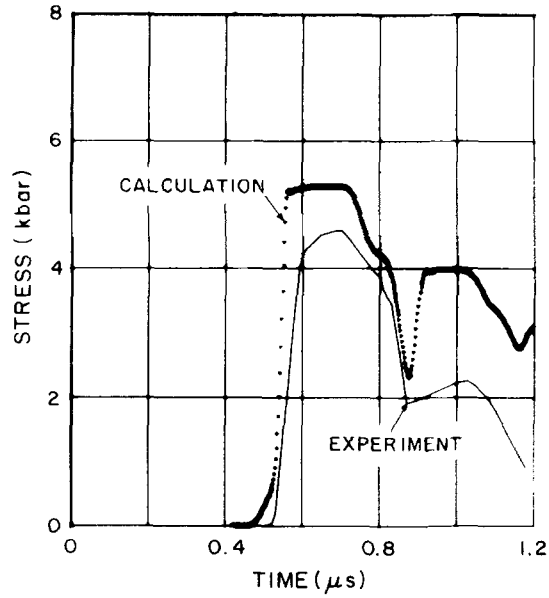

FIG. 6. Measured response for spall fracture in copper compared with simple tensile fracture model. The mean stress to produce fracture is taken as -18 kbars.

Time-independent criteria are not sufficient to represent the experimental data shown in Fig. 5. A calculation of this experiment is shown in Fig. 6 for time-independent spall strength of 18 kbars.

Application of the dynamic hole growth analysis to the problem of time-dependent spallation in copper gives very good representation of the data (as shown in Fig. 7) with the material parameters listed in Table I.

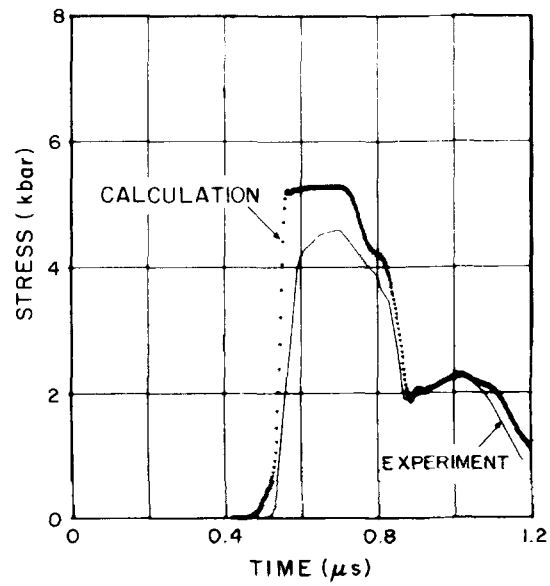

FIG. 7. Measured response for spall fracture in copper compared with rate-dependent ductile hole-growth model ($\tau = 0.054$ μs). Calculations with $\tau = 0$ and 0.100 μs give identical results.

TABLE I. Material parameters for spallation and fragmentation calculations.

	Copper	PMMA [a]	A533B Steel
$\bar{\rho}_0$	8.924 g/cm^3	1.184 g/cm^3	7.890 g/cm^3
c_0	0.391 cm/μs	0.276 cm/μs	0.458 cm/μs
s	1.51	2.5	1.50
$\bar{\Gamma}_0$	2.0		2.0
Y_0	1.5 kbars		5.5 kbars
G_0	484 kbars		790 kbars
α_0	1.0003		1.0006
a_s	1.7 kbars		
τ	0.054		
η	10 P		

[a]PMMA is treated in these calculations as a fluid (no shear strength), but with the longitudinal sound speed of 0.276 cm/μs substituted for the bulk velocity c_0.

The initial distention $\alpha_0 = 1.0003$ is taken to be the measured porosity in the recovered sample at locations far from the spall plane: the actual porosity prior to shock loading was not reported.[18] The parameter τ is determined from Eq. (13) and the measured void number density (10^7 cm^{-3}) at points far from the spall plane. This gives an average initial pore radius $a_0 = 0.00019$ cm and value of $\tau = 0.054$ μs.

Two independent calculations were performed for $\tau = 0$ and $\tau = 0.100$ μs with the result that the computed pressure histories were indistinguishable from the $\tau = 0.054$ μs case (Fig. 7). Thus the abbreviated and simplified hole-growth model represented by Eqs. (32) can be used without loss of accuracy in describing the physical process.

The calculated peak amplitude shown in Fig. 7 does not agree with the measured value. The same problem was encountered by Seaman *et al.*[18] and may have to do with the experimental measurement itself or with the equation of state used for PMMA. In any event, the measured *spall signal* is believed to be accurate, and no attempt is made to "force" the maximum stress amplitude into better agreement with the data.

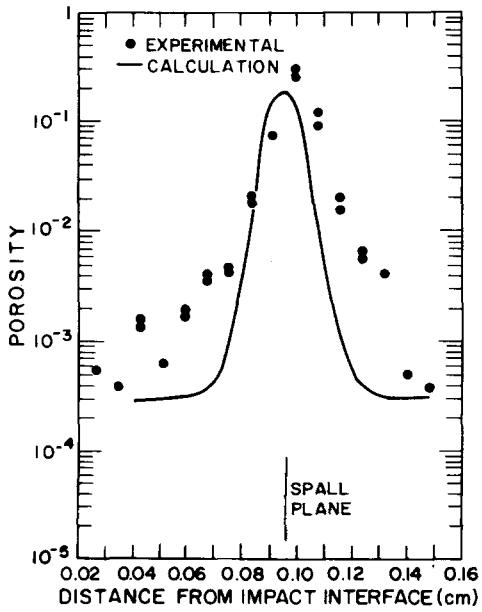

FIG. 8. Comparison of calculated (solid line) and measured (data points) postimpact porosity in copper sample (SRI-S24).

Comparison of the calculated final porosity, or void volume, with experimental measurement is shown in Fig. 8. The calculated distribution is narrower than measured, particularly for porosities less than 1%, but the overall agreement is reasonably good.

An unexpected result of these calculations is the small value of η that is required to reproduce the measured spall signal in Fig. 7. The "viscosity" of metals (i.e., the maximum resolved shear stress divided by the *plastic* shear strain rate in states of rapid plastic deformation) is usually found to be on the order of anywhere from 10^3 to 10^5 P for conditions of homogeneous compressive deformation.[27–29] For heterogeneous plastic deformation there exists substantial localized heating effects. Plastic shear strains of several thousand percent are developed at the expanding pore walls. The magnitude of the corresponding temperature change can be estimated by calculating the plastic shear strain γ^p at the pore wall ($r = a$) from Eqs. (8a) and (24):

$$\gamma^p = \epsilon_r - \epsilon_\theta = -\left(\frac{\alpha_0 - 1}{\alpha - 1}\right)^{-2/3} + \left(\frac{\alpha_0 - 1}{\alpha - 1}\right)^{1/3}. \quad (44)$$

Since plastic deformation is assumed to take place at constant shear stress ($\sigma_r - \sigma_\theta = -Y_0$), the plastic work per unit mass done at the expanding pore wall is $W_p = -Y_0\gamma^p/\rho_0$. For $\alpha_0 = 1.0003$ and $\alpha = 1.1$ (expansion to 10% porosity), $\rho_0 = 8.9$ g/cm^3, and $Y_0 = 0.0015$ Mbar, $\gamma^p = 48$ and $W_p \cong 200$ cal/g. If it is assumed that all the plastic work goes into heating, and the specific heat is taken to be 0.3 cal/g K, then $\Delta T \cong 670$ K. Thus the temperature at the expanding pore wall can be a substantial fraction of the melting temperature. It is not quantitatively known what effect this has on the relationship between plastic shear strain rate and applied shear stress, but there presently exist no data that precludes the possibility of a value of $\eta = 10$ P in the heterogeneous spallation and void growth process envisioned here. Seaman *et al.*[18] also found that a value of $\eta (\sim 75$ P) slightly lower than expected was required for the NAG model to reproduce these data on copper, but did not speculate on possible sources of this low value.

Tensile stresses generated by detonation of a high explosive[4,5,7] in contact with a metal are much greater than usually studied by plate-impact techniques. Also, as outlined in the introduction, the fracture process is considerably more complicated than in the plate-impact configuration since the spall location becomes one of the variables in addition to the spall strength.

To show the rather remarkable generality of the foregoing model of dynamic ductile fracture of copper, as determined by a single plate-impact experiment, a calculation is made of explosively produced spall fracture in copper as observed by the Los Alamos Scientific Laboratory flash-radiographic facility PHERMEX.[30] Figure 9 shows a flash radiograph of 25-mm-thick copper plate in contact (below, not shown) with a 12.7-mm-thick piece of composition B-3 initiated with a P-40 lens (PHERMEX Shot 500, Ref. 30). The

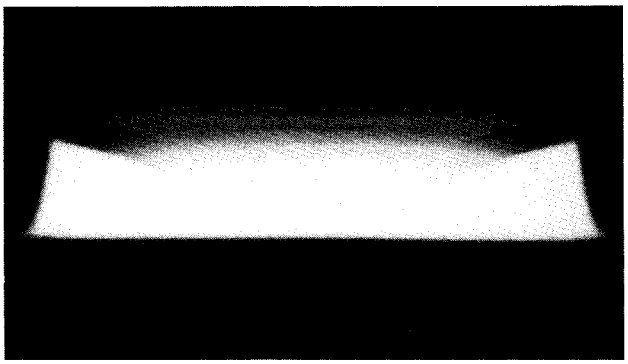

FIG. 9. X radiograph (LASL PHERMEX Shot 500) of spalling copper sample (25 mm thick) in contact with 12.7-mm composition B-3. The detonated explosive (not shown) lies below the copper sample. Two distinct spall layers are seen: 2 and 3 mm thick.

radiograph is taken at a time of 27.6 μs after explosive initiation and shows two distinct spall planes—the first (at the top, closest to the free surface) plane is approximately 2 mm thick and the second plane is approximately 3 mm thick. Calculation of the loading history on the copper sample was performed by Mader with the numerical finite-difference code SIN[31] which contains the necessary explosive burn routines. With the known loading history, a spallation calculation is made using the same pore-growth model used for the plate-impact experiment of Fig. 7: The material parameters remain exactly the same, only the loading conditions are changed. The results of this calculation are shown in Fig. 10 at successive times following first application of the SIN-calculated stress history at a point 1 cm from the free surface.

At $t = 2.0\,\mu$s, the triangular-shaped particle-velocity pulse is just about to reflect from the free surface (1 cm from the left boundary). At 3.0 μs, the pulse has reflected, the particle velocity at the free surface has approximately doubled, and the porosity has just begun to grow (maximum at ~ 1 mm from the free surface). The porosity continues to grow until two rather distinct humps are formed at 2 and 5 mm from the free surface. When the porosity reaches 30%, it is assumed that additional ductile hole growth is halted by brittle fracture between individual voids and complete spall ensues, as indicated by the two spikes in the porosity curve at $t = 5.3\,\mu$s.

The material between these two planes is still being pulled in tension at $t = 5.3\,\mu$s, as indicated by the positive velocity gradient. Therefore additional fracturing should occur in this layer. This is indeed the case as shown in Fig. 11 ($t = 6.0\,\mu$s), where a region about 2 mm thick is continually fractured, but the major discontinuities in particle velocity are at the two initial spall planes. Therefore one would predict that two distinct spall layers would be seen, one 2 mm thick, closest to the free surface, and the second 3 mm thick. This, of course, is what is observed experimentally in Fig. 9.

It is quite remarkable that the pore-growth model, whose parameters were derived from the plate-impact data at a peak tensile stress of ~ 15 kbars, would work so well in representing dynamic ductile fracture for tensile stresses approaching 100 kbars. In addition to simply giving the correct

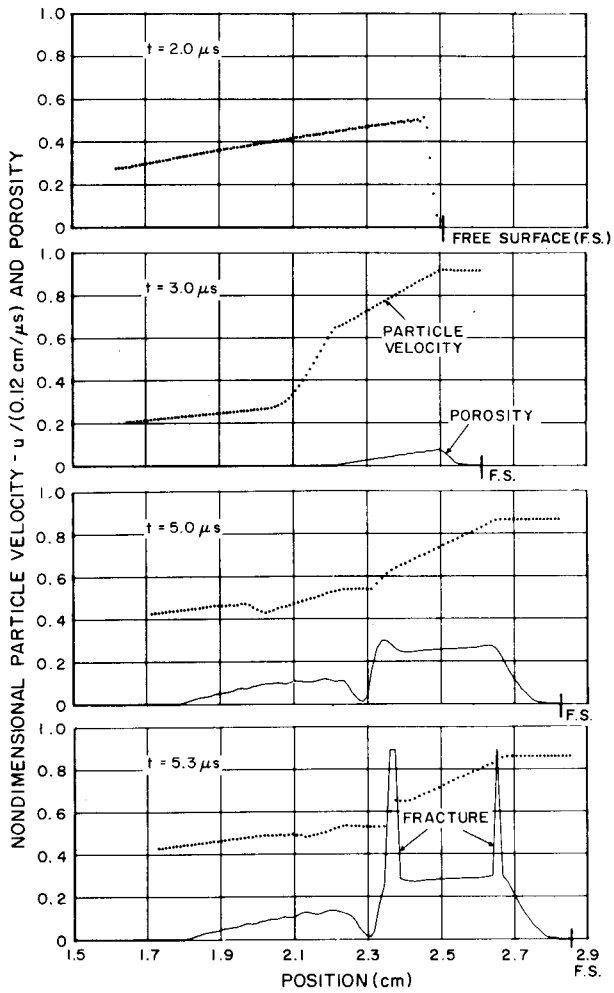

FIG. 10. Calculated particle velocities and porosities for LASL PHERMEX Shot 500 based on ductile hole-growth model with material parameters obtained from plate-impact test (SRI-S24).

spall thicknesses, the theoretical calculation shows the unusual way in which the porosity changes with time. Simple heuristic models of explosively induced spall (as discussed in the introduction) picture multiple spall fracture originating

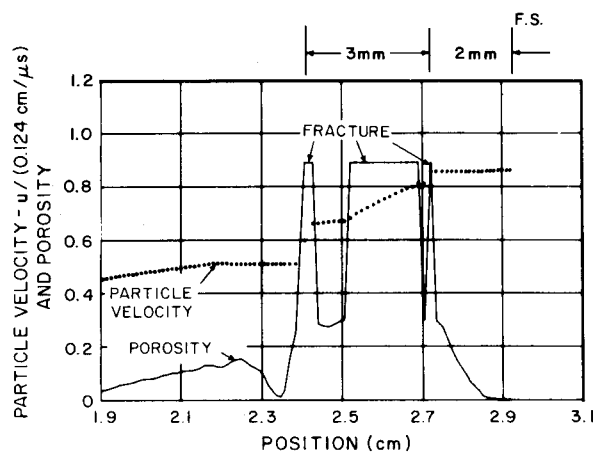

FIG. 11. Final calculated fracture and porosity distribution for LASL PHERMEX Shot 500. The region between the two visible spall planes (i.e., those with particle velocity discontinuities) continues to break up after spall plane formation.

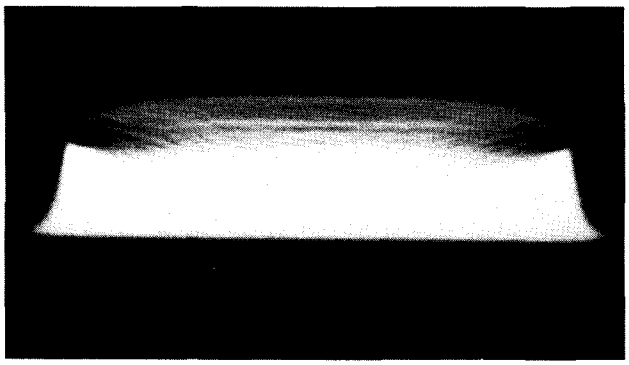

FIG. 12. X radiograph (LASL PHERMEX Shot 464) of spalling copper sample (25 mm thick) in contact with 25 mm of composition B-3. Note the "wispy," fractured nature of the material behind the first spall plane.

first near the free surface and progressing back into the solid. The pore-growth model calculation presented here shows the second spall plane (at 5 mm from the free surface) as occurring first.

Also, the calculation shows a multiply fractured segment between the two spall planes while the radiograph of Fig. 9 does not. However, it is found experimentally that a change of the explosive thickness from 12.7 to 25.4 mm gives the result shown in Fig. 12 (PHERMEX Shot 464, Ref. 30). Here, the material between the two spall planes appears to be multiply fractured in almost *exactly* the way predicted by the pore-growth fracture model (see Fig. 11).

These results are a consequence of, and highly sensitive to, the loading history applied by the high explosive. This is something that is calculated rather than measured, and therefore detailed conclusions about the way in which materials fracture must be postponed until adequate measurement of these loading conditions are determined experimentally.

Nevertheless, it is obvious that the theory presented here goes a long way in unifying the low-pressure (plate-impact) and high-pressure (explosive loading) spallation data.

V. DYNAMIC FRACTURE OF EXPANDING RINGS

Based on the dynamic ductile fracture properties of copper, determined in the previous section, and similar properties for A533B pressure-vessel steel, the fracture of expanding metal rings is now considered.

For an initial distention of $\alpha_0 = 1.0003$ and a value of $a_s = 1.7$ kbars, void growth in copper begins at a mean tensile stress given by Eq. (32); i.e.,

$$P_{\text{eq}} = -\frac{a_s}{\alpha_0}\ln\frac{\alpha_0}{\alpha_0 - 1} = -13.8 \text{ kbars}.$$

For an expanding ring, with only one nonzero principal stress component, $\bar{\sigma}_{\theta\theta}$, the mean tensile stress is $\frac{1}{3}\bar{\sigma}_{\theta\theta}$. Therefore ductile hole growth in an expanding copper ring would not begin until $\bar{\sigma}_{\theta\theta}$ reached 41 kbars, which is very likely impossible. Because of homogeneous plastic shear deformation in the absence of work-hardening, $\bar{\sigma}_{\theta\theta}$ is limited to Y_0 which is on the order of a kilobar or so. Even in the presence of substantial work-hardening, it is unlikely that the yield strength would increase as much as 40 kbars.

In the case of spallation under conditions of uniaxial strain, the stress state is predominantly hydrodynamic with a relatively small, superimposed deviatoric component. Homogeneous plastic shear deformation under conditions of uniaxial strain cannot limit the magnitude of the mean tensile stress as it can in a simple uniaxial-stress tensile experiment. Thus the ductile fracture model based on growth of spherical voids under the influence of a mean tensile stress does not apply to fracture of expanding rings. One might think that this should have been obvious from the start, but that is not true. This conclusion stems from the fact that $|3P_{\text{eq}}| \gg Y_0$. If $|3P_{\text{eq}}| < Y_0$, spherical hole growth according to the model presented here would have been theoretically possible.

The new theory that is needed in one which describes the plastic growth of voids under combined mean and deviatoric stress conditions. The case of pure hydrodynamic stress state would then simply be a special case, and spallation would also be encompassed by the more general analysis. Shockey *et al.*[32] propose a method of doing this for void growth in uniaxial tension by using a mathematical result of Rice and Tracey[33] for the expansion of spherical voids in a nonhydrostatic stress field. This analysis gives $\dot{a}/a$ (see Fig. 3) in terms of the mean stress and shear stress as $r \to \infty$.

Instead of applying this result to the problem of an expanding ring, a purely phenomenological approach is used here. This is based on the data of Shockey *et al.*[32] for the

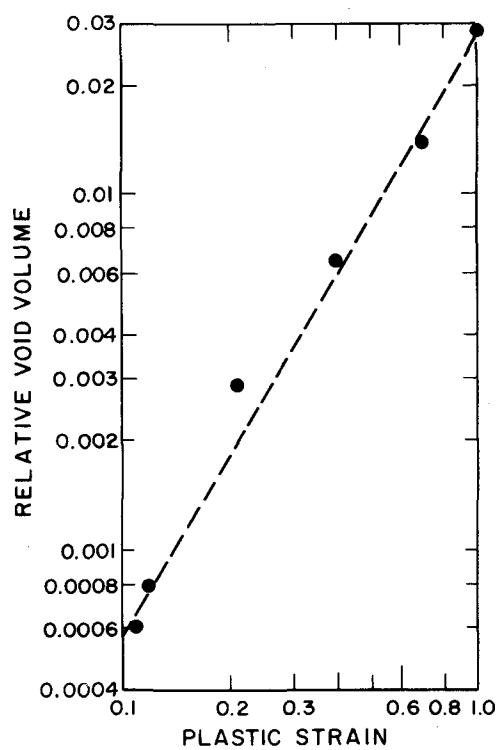

FIG. 13. Experimentally determined variation in relative void volume (porosity) and longitudinal plastic strain for A533B pressure-vessel steel subject to uniaxial tensile loading. Catastrophic void coalescence and fracture occurs at a porosity of 3%.

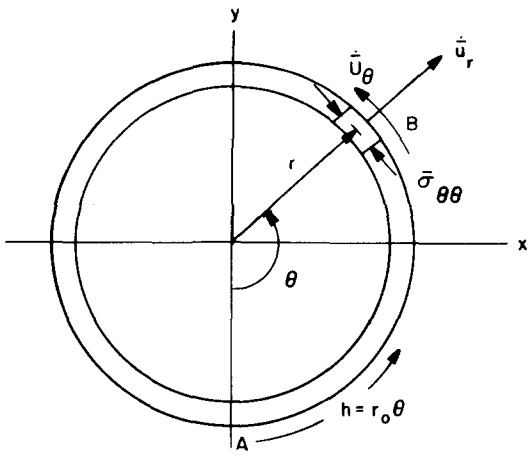

FIG. 14. Ring geometry. The origin for the equivalent one-dimensional system is point A. The initial radius is r_0.

ductile fracture of A533B pressure-vessel steel. In simple tensile rupture experiments it is found that the fractional void volume (or plastic volume strain) is approximately $\bar{\epsilon}_v^p = 0.0006$ at a longitudinal plastic strain of $\psi^p = 0.11$. The longitudinal plastic strain ψ^p is related to the shear strain γ^p, defined previously, according to $\gamma^p = \frac{1}{2}\psi^p$. The plastic volume strain is a linear function of ψ^p on a log-log scale up to $\bar{\epsilon}_v^p = 0.03$ and $\psi^p = 1.0$, at which point the material fails catastrophically. The experimental data are shown in Fig. 13.

For fracture and fragmentation in an expanding ring, one is interested in wave propagation around the circumference. Thus it is convenient to cast the nearly radially symmetric two-dimensional ring problem in a one-dimensional form.

The equations of motion for an expanding ring of radius r (initial radius r_0) with single nonzero stress component $\bar{\sigma}_{\theta\theta}$ as a function of θ only (see Fig. 14) are

$$\bar{\rho}\frac{d\dot{\bar{u}}_\theta}{dt} = -\frac{1}{r}\left(\frac{\partial\bar{\sigma}_{\theta\theta}}{\partial\theta}\right)_t, \tag{45}$$

$$\bar{\rho}\frac{d\dot{\bar{u}}_r}{dt} = \frac{\bar{\sigma}_{\theta\theta}}{r}, \tag{46}$$

where the total time derivatives in Eqs. (45) and (46) represent the acceleration components of a material element. Equation (45) gives the acceleration in the circumferential direction due to wave propagation around the ring circumference, while Eq. (46) gives the radial acceleration due to hoop forces.

To translate Eqs. (45) and (46) to an equivalent one-dimensional problem, a Lagrangian circumferential coordinate h is defined in terms of the initial radius r_0 according to $h = r_0\theta$. Point A in Fig. 14 is arbitrarily chosen as the material element $h = 0$, and the initial length of the one-dimensional system is $2\pi r_0$. Conservation of mass requires that

$$\bar{\rho}_0 A_0 r_0\, d\theta = \bar{\rho} A r\, d\theta, \tag{47}$$

where A is the cross-sectional area of the ring and subscript 0 refers to initial conditions. With these definitions, Eqs. (45) and (46) can be written in Lagrangian form as

$$\bar{\rho}_0\left(\frac{\partial\dot{\bar{u}}_\theta}{\partial t}\right)_h = -\frac{A}{A_0}\left(\frac{\partial\bar{\sigma}_{\theta\theta}}{\partial h}\right)_t, \tag{48}$$

$$\bar{\rho}_0\left(\frac{\partial\dot{\bar{u}}_r}{\partial t}\right)_h = \frac{A}{A_0}\frac{\bar{\sigma}_{\theta\theta}}{r_0}. \tag{49}$$

As the ring is driven outward, the material is being strained in the circumferential direction as a result of two effects: a strain rate $\dot{\bar{u}}_r/r$ due to outward radial motion and a contribution $(1/r)\partial\dot{\bar{u}}_\theta/\partial\theta$ due to circumferential motion. If a velocity $\dot{\bar{u}}$ is defined as

$$\dot{\bar{u}} = \theta\langle\dot{\bar{u}}_r\rangle + \dot{\bar{u}}_\theta, \tag{50}$$

where $\langle\dot{\bar{u}}_r\rangle$ is the circumferential average of $\dot{\bar{u}}_r$ and therefore independent of θ,

$$\frac{1}{r}\frac{\partial\dot{\bar{u}}}{\partial\theta} = \frac{\langle\dot{\bar{u}}_r\rangle}{r} + \frac{1}{r}\frac{\partial\dot{\bar{u}}_\theta}{\partial\theta}. \tag{51}$$

Therefore the velocity function $\dot{\bar{u}}$ in Eq. (50) contains both the effect of average radial straining and the circumferential motion. From Eqs. (48)–(50) one can then write

$$\bar{\rho}_0\left(\frac{\partial\dot{\bar{u}}}{\partial t}\right)_h = -\frac{A}{A_0}\left(\frac{\partial\bar{\sigma}_{\theta\theta}}{\partial h}\right)_t + \frac{h}{r_0^2}\left\langle\frac{A\bar{\sigma}_{\theta\theta}}{A_0}\right\rangle \tag{52}$$

for the equivalent one-dimensional system describing the motion of a ring. The first term on the right-hand side of Eq. (52) is the driving force for circumferential motion, while the second term is an acceleration term due to the average hoop stress around the circumference. Initial conditions on the velocity variable u are obtained from a known initial outward velocity V and Eq. (50): $\dot{\bar{u}}(h,0) = hV/r_0$.

The elastic-plastic stress-strain relationship for an expanding ring undergoing homogeneous plastic shear deformation and void growth is written as

$$\dot{\bar{\sigma}}_{\theta\theta} = \bar{E}(\dot{\bar{\epsilon}} - \dot{\bar{\epsilon}}^p_{\theta\theta}), \tag{53}$$

where $\bar{E}$ is Young's modulus of a porous material element and $\dot{\bar{\epsilon}}$ is the total strain rate $-(\partial\dot{\bar{u}}/\partial h)_t$ in the equivalent one-dimensional system. The plastic strain-rate tensor is of the form

$$\dot{\bar{\epsilon}}^p = \begin{bmatrix} -\dot{\alpha}/3\alpha & 0 & 0 \\ 0 & -\dot{\alpha}/3\alpha & 0 \\ 0 & 0 & -\dot{\alpha}/3\alpha \end{bmatrix} + \begin{bmatrix} \dot{\psi}^p & 0 & 0 \\ 0 & -\frac{1}{2}\dot{\psi}^p & 0 \\ 0 & 0 & -\frac{1}{2}\dot{\psi}^p \end{bmatrix}, \tag{54}$$

in a coordinate system such that x_1 is in the circumferential direction and x_2 and x_3 are the mutually perpendicular transverse directions. The first matrix in Eq. (54) represents the porosity change and the second represents homogeneous plastic shear deformation. The total volumetric plastic strain rate is $-\dot{\alpha}/\alpha$ which comes solely from the first matrix on the right-hand side of Eq. (54). Thus Eq. (53) becomes

$$\dot{\bar{\sigma}}_{\theta\theta} = \bar{E}(\dot{\bar{\epsilon}} + \dot{\alpha}/3\alpha - \dot{\psi}^p). \tag{55}$$

If the material under consideration is elastic-perfectly plas-

tic (constant yield strength Y_0), then $\bar{\sigma}_{\theta\theta} = Y_0/\alpha$ during plastic flow, i.e., the yield strength is reduced by the factor $1/\alpha$ as a result of material porosity. Therefore an additional expression must be satisfied when plastic void growth occurs:

$$\dot{\bar{\sigma}}_{\theta\theta} = -(Y_0/\alpha)(\dot{\alpha}/\alpha). \tag{56}$$

Finally, experimental data of Shockey *et al.* is used to give $\dot{\psi}^p$ in terms of $\dot{\alpha}$, α, and ψ^p. A plot of the relative void volume $-\bar{\epsilon}_v = \ln\alpha$ as a function of ψ^p for uniaxial-stress tension on A533B pressure-vessel steel is a straight line on a log-log graph, Fig. 13. Thus

$$\frac{d\ \ln(\ln\alpha)}{d\ \ln\psi^p} = k \tag{57}$$

or

$$\dot{\alpha} = k\alpha\ \ln\alpha\frac{\dot{\psi}^p}{\psi^p}. \tag{58}$$

Below a value of $\psi^p = 0.11$, the plastic volume strain is assumed to be constant at 0.0006. From $\psi^p = 0.11$ to 1.0, Eq. (58) applies with $k = 1.74$. At $\psi^p = 1.0$, or $-\ln\alpha = 0.03$, catastrophic fracture occurs.

Therefore Eqs. (55), (56), and (58), when integrated, give $\bar{\sigma}_{\theta\theta}$, α, and ψ^p for a known strain-rate history $\dot{\bar{\epsilon}} = -(\partial\dot{\bar{u}}/\partial h)_t$. These equations are combined with Eq. (52) and solved numerically with an initial random distribution for the distension α to give the fragmentation response of an A533B steel ring. The statistical distribution of the distension is given in the Appendix. In the sample problems it is assumed that the cross-sectional area is initially uniform and that changes are small. It is also assumed that the initial radius is large enough to neglect the second term on the right-hand side of Eq. (52). The thermomechanical properties of steel that are used in this problem are given in Table I.

The results of these calculations for four independent samplings of the random variable ϕ (from which the initial distention α_0 is determined) defined in the Appendix are shown in Fig. 15. The steel ring (of initial circumference $2\pi r_0 = 16$ cm) is given an initial outward velocity of $V = 0.01$ cm/μs, and $nA = 10^7\ \text{cm}^{-1}$. The finite-difference calculation is performed with 100 zones and $\Delta h = 0.16$ cm. Fracture occurs at elements that reach a relative void volume, or porosity, of 0.03. This occurs at a time of approximately 1.7 ms when the circumference has reached a value of ~ 33 cm. The final porosity in the unfractured elements generally lies between 0.029 and 0.030; i.e., all computational zones are close to the point of fracture at the time of fragmentation when the circumferential stress is relieved.

The four calculations shown in Fig. 15 (clockwise starting from the upper left-hand corner) resulted in 4, 2, 5, and 3 intact segments or fragments as a result of the four independent random samplings of initial distention α_0. This is similar to experimental studies of radial fracture and fragmentation in which one cannot reproduce exactly the same number of fragments in identical experiments, but only a statistical distribution.

The calculated fragment distribution of Fig. 15 is due to the statistical variation in initial porosity and the assumption

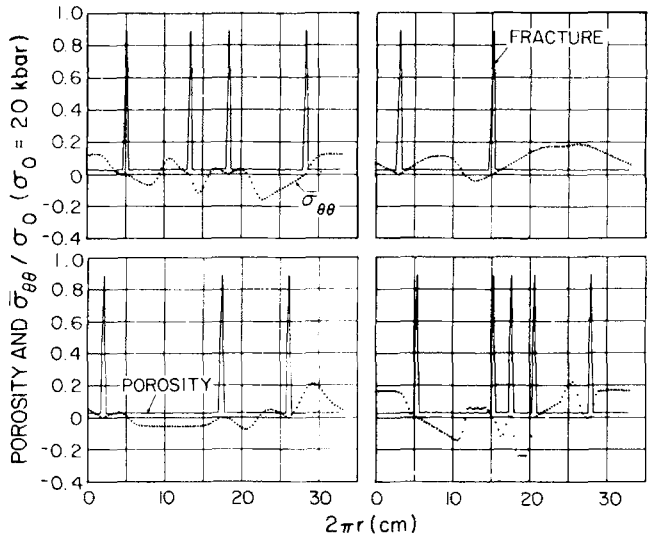

FIG. 15. Calculated hoop stress, porosity, and fracture locations for impulsively loaded steel ring. The only difference between the four calculations is in initial porosity assigned to each volume element according to the statistical distribution given in the Appendix.

that ductile void growth is the mechanism of failure. It is often observed that ductile fracture of expanding rings is preceded by necking, possibly due to a combination of initial porosity and variation in cross-sectional area.[34] The latter effect has been completely ignored in the computations shown here. However, it would be possible to include if information were available on the variation in cross-sectional area due to the particular fabrication process. Taylor *et al.*[23] considered the instability in stretching plates and shells due to variation in shell thickness. The theory was based on the formalism of hydrodynamics and neglected random material property effects such as initial porosity and ductile hole growth. A combination of the effects of area variation and porosity distribution would perhaps lead to a physically more realistic description of the phenomenon of dynamic fracture of rings. This remains to be investigated.

Another important effect that has been ignored here is that of adiabatic shear banding; this is the localization of plastic shear deformation $\gamma^p = \frac{3}{2}\psi^p$ to a number of heterogeneous regions of extremely large inelastic strain rather than the homogeneous deformation process treated here. The possible occurrence of adiabatic shear banding depends on a number of material properties: (i) low thermal conductivity, (ii) low work-hardening coefficient, and (iii) a substantial decrease in the flow stress with increasing temperature. For materials in which adiabatic shear banding occurs, the fragmentation process will differ from the ductile hole growth model presented here, and a modified theory will be constructed. One of the necessary ingredients of such a theory is quantification of the type of flaw that leads to shear instability. These flaws have not yet been identified.[35]

The calculations for A533B stainless steel that are shown here illustrate the *kind* of statistical treatment that can be undertaken to describe fracture and fragmentation of rings and shells. The development of a genuine quantitative theory that works for a range of materials and experimental

loading conditions will require pre- and postshot microstructural examination and identification of the actual flaws which lead to instability and the resulting fracture.

VI. SUMMARY

A ductile hole-growth model is developed which works well in describing spall fracture of copper for plate-impact and explosive loading conditions. Previous models have been found to work well in the incipient stages of ductile fracture,[16–19] while others seem to be more applicable to complete separation.[15] One of the major differences in the model proposed here, as compared to other microscopic descriptions of ductile hole growth,[16,18] is the fact that the mean tensile stress around a single pore is applied at a finite radius determined by Eq. (3). This leads directly to a threshold mean stress as a function of the current distention, Eq. (29), analogous to the "strength function" of Cochran and Banner.[15] This description thus tends to bridge the gap between the low-damage and complete separation regimes of spall fracture.

In particular, material parameters describing plate-impact spallation in copper work well in reproducing measured spall thicknesses in explosively loaded samples. The "spall gradient" model[7] also gives the correct spall thickness, but does so because it is simply forced to. In the PHERMEX experiments a spall thickness δ_s is measured radiographically; this is the *only* experimental measurement. The maximum tensile mean stress $-\bar{p}_s$ at the spall plane is then *calculated*.[7] It is found that below the ultimate spall pressure $\bar{p}_{\max}$ (on the order of 10^2 kbars for most materials) a plot of $\bar{p}_s$ vs $(\bar{p}_s/\delta_s)^{1/2}$ forms a straight line. Therefore the spallation criterion defined by $(-\bar{p}) = [(-\bar{p})/\delta]^{1/2}$ (for $-\bar{p} < \bar{p}_{\max}$) is absolutely guaranteed to give back the measured spall thickness δ_s. The ductile hole-growth model presented here actually predicts the locations of material separation and porosity near the spall plane. The agreement with the PHERMEX radiographs is somewhat remarkable in view of the approximate method used to reproduce the explosive loading conditions. If additional work were to be done in the area of explosively produced spallation, it would be necessary to actually measure the loading history rather than relying totally on calculation.

The influence of internal gas pressure has been included in the formal theory of ductile hole growth, but no calculations were performed on spall fracture in reactive solids. Wackerle and Anderson[36] have studied the problem of explosive initiation in shock compression using an analysis similar to the one given here. Additional research is necessary to quantify the effect of pore pressure on dynamic tensile fracture in reactive media.

As was stated in the introduction, one of the goals of this work was to relate spallation information and data to the fracture of expanding rings and shells. This was not achieved. Uniaxial-strain conditions associated with spallation produce a stress state which is predominantly isotropic with a smaller deviatoric effect added on. Therefore the ductile hole-growth model based on mean tensile stress alone is applicable.

In the case of expanding rings, the mean stress $\frac{1}{3}\bar{\sigma}_{\theta\theta}$ and the circumferential deviatoric stress $\frac{2}{3}2\bar{\sigma}_{\theta\theta}$ are not independent and are of the same order of magnitude. Also, large homogeneous plastic shear strains precede hole growth in the expanding ring; consequently, a model describing ductile hole growth will have to include homogeneous shear deformation as well as nonisotropic stress fields. This paper presents a phenomenological description of ductile fracture of an expanding ring. The essential ingredients of the *kinds* of things that must be included in such a theory are given here. These include identification and quantification of the dominant flaws that eventually grow to produce a fracture, and the appropriate one-dimensional differential equation describing circumferential wave propagation (including initial conditions) of an expanding ring, Eq. (52).

Some attempt has already been made to develop ductile fracture models for more general nonisotropic stress and strain states.[32,33,37] By continuing this line of investigation theoretically, complemented by careful experimental measurement and microscopic observation, the connection between the fracture of expanding rings (by means of ductile hole growth, adiabatic shear banding, brittle failure, or other) and spallation can eventually be made.

ACKNOWLEDGMENTS

The author wishes to acknowledge the following people for their numerous and helpful technical contributions in the course of this work: C. L. Mader and R. D. Dick (Los Alamos Scientific Laboratory), Lynn Seaman (SRI international), S. G. Cochran (Lawrence Livermore Laboratory), and L. W. Davison (Sandia Laboratories).

APPENDIX

The initial porosity ϕ or distension $\alpha = 1/(1-\phi)$ is a random variable which depends on the volume of the material element being considered. Let $\bar{\phi}$ be the average porosity of a representative sample containing a very large number of voids. As one samples smaller and smaller elements, the statistical chance for significant departure from $\bar{\phi}$ increases. Poisson statistics are used to obtain a statistical distribution of ϕ.

Let the porosity be due to a large number of small voids, n per unit volume, each of the same size (radius a_0) and randomly distributed throughout the sample. Let the average porosity of the entire sample by $\bar{\phi}$. If the total volume V is divided into a number of elements each of volume ΔV, then the probability of the volume ΔV containing at least j voids is given by the Poisson distribution[38]:

$$P(j,\Delta V) = e^{-n\Delta V}\sum_{i=0}^{j}\frac{(n\Delta V)^i}{i!}. \tag{A1}$$

The number j is related to the porosity ϕ according to

$$j = 3\phi\Delta V/4\pi a_0^3. \tag{A2}$$

For large $n\Delta V$ the Poisson distribution approaches the normal distribution with expectation $n\Delta V$ and variance, $n\Delta V$[38]

i.e.,

$$P(j,\Delta V)\cong\frac{1}{\sqrt{\pi}}\int_{-\infty}^{u} e^{-z^2}dz, \tag{A3}$$

where

$$u=\frac{j-n\Delta V}{(2n\Delta V)^{1/2}}=\left(\frac{n\Delta V}{2}\right)^{1/2}\left(\frac{\phi-\bar{\phi}}{\bar{\phi}}\right), \tag{A4}$$

where $\bar{\phi}=\frac{1}{3}4\pi a_0^3 n$. Thus the probability that the porosity is less than or equal to ϕ in a volume element ΔV can be obtained from the normal random variable u, with expectation 0 and unit variance (this is generated numerically with a random number routine), and Eq. (A4) according to

$$\phi=\bar{\phi}\left(1+\left(\frac{2}{n\Delta V}\right)^{1/2}u\right). \tag{A5}$$

If one-dimensional finite-difference calculations are being performed, $\Delta V=A\Delta h$, where A is the cross-sectional area of the ring and Δh is the Lagrangian step size. Therefore, for smaller and smaller Δh, the departure of ϕ from the average $\bar{\phi}$ increases. This is an important consideration in any mathemathetical model of statistical fracture or fragmentation.

One might argue that not all of the holes are the same size, and additional considerations are necessary. Future statistical analyses can take these effects into account.

[1]B. Hopkinson, Trans. R. Soc. London **213A**, 437 (1914).
[2]J. S. Rinehart, J. Appl. Phys. **22**, 555 (1951).
[3]J. S. Rinehart, J. Appl. Phys. **23**, 1229 (1952).
[4]J. S. Rinehart and J. Pearson, *Behavior of Metals Under Impulsive Loads* (American Society for Metals, Cleveland, 1954).
[5]R. G. McQueen and S. P. Marsh, J. Appl. Phys. **33**, 654 (1962).
[6]I. C. Skidmore, Appl. Mater. Res. **4**, 131 (1965).
[7]B. R. Breed, C. L. Mader, and D. Venable, J. Appl. Phys. **38**, 3271 (1967).
[8]J. H. Smith, *Dynamic Behavior of Materials, ASTM Materials Science Series*—5, *Special Publication No.* 336 (American Society for Testing Materials, Philadelphia, 1963) pp. 264–281.
[9]B. M. Butcher, L. M. Barker, D. E. Munson, and C. D. Lundergan, AIAA J. **2**, 977 (1964).
[10]F. R. Tuler and B. M. Butcher, Int. J. Fract. Mech. **4**, 431 (1968).
[11]A. L. Stevens and F. R. Tuler, J. Appl. Phys. **42**, 5665 (1971).
[12]L. Davison and A. L. Stevens, J. Appl. Phys. **43**, 988 (1972).
[13]A. L. Stevens, L. Davison, and W. E. Warren, J. Appl. Phys. **43**, 988 (1972).
[14]L. Davison, A. L. Stevens, and M. E. Kipp, J. Mech. Phys. Solids **25**, 11 (1977).
[15]S. Cochran and D. Banner, J. Appl. Phys. **48**, 2729 (1977).
[16]T. W. Barber, L. Seaman, R. C. Crewdson, and D. R. Curran, J. Mater. **7**, 393 (1972).
[17]D. R. Curran, D. A. Shockey, and L. Seaman, J. Appl. Phys. **44**, 4025 (1973).
[18]L. Seaman, T. W. Barbee, Jr., and D. R. Curran, Stanford Res. Inst. Tech. Report No. AFWL-TR-71-156, Dec. 1971 (unpublished).
[19]D. R. Curran, L. Seaman, and D. S. Shockey, Phys. Today **30**, 46 (1977).
[20]C. L. Mader (private communication).
[21]N. F. Mott, Proc. R. Soc. London **189**, 300 (1947).
[22]D. L. Wesenberg and M. J. Sagartz, J. Appl. Mech. **44**, 643 (1977).
[23]J. W. Taylor, F. H. Harlow, and A. A. Amsden, J. Appl. Mech. **45**, 105 (1978).
[24]M. M. Carroll and A. C. Holt, J. Appl. Phys. **43**, 1626 (1972).
[25]T. Vreeland, Jr. and K. M. Jassby, in *Metallurgical Effects at High Strain Rates*, edited by R. W. Rohde, B. M. Butcher, J. R. Holland, and C. H. Karnes (Plenum, New York, 1973), pp. 277–284.
[26]J. H. Mackenzie, Proc. Phys. Soc. **63B**, 2 (1950).
[27]S. K. Godunov, A. A. Deribas, and V. I. Mali, Combust. Explos. Shock Waves USSR **11**, 1 (1975).
[28]F. E. Prieto and C. Renero, J. Appl. Phys. **44**, 4103 (1975).
[29]L. C. Chhabildas and J. R. Asay, J. Appl. Phys. **50**, 2749 (1979).
[30]C. L. Mader, T. R. Neal, and R. D. Dick, *LASL Phermex Data* (University of California, Berkeley, 1980), Vol. I and II.
[31]C. L. Mader, *Numerical Modeling of Detonations, Los Alamos Series in Basic and Applied Sciences*, edited by D. H. Sharpe and L. M. Simmons, Jr. (University of California, Berkeley, 1979).
[32]D. A. Shockey, L. Seaman, K. C. Dao, and D. R. Curran, J. Pressure Vessel Technol. **102**, 14 (1980).
[33]J. R. Rice and D. M. Tracey, J. Mech. Solids **13**, 201 (1969).
[34]A. E. Carden (private communication).
[35]D. A. Shockey and D. C. Erlich, in *Metallurgical Effects of High Strain Rate Deformation and Fabrication*, edited by M. A. Meyers and L. E. Murr (Plenum, New York, to be published).
[36]J. Wackerle and A. B. Anderson, Bull. Am. Phys. Soc. **24**, 718 (1979).
[37]A. L. Gurson, J. Eng. Mater. Technol., Trans. of ASME **99**, 2 (1977).
[38]Z. W. Birnbaum, *Introduction to Probability and Mathematical Statistics* (Harper, New York, 1962), p. 153.